Studying highly relativistic vortex-electron beams by atomic scattering

V. K. Ivanov ©,* A. D. Chaikovskaia ©, and D. V. Karlovets ©

School of Physics and Engineering, ITMO University, 197101 St. Petersburg, Russia

We explore the opportunities of using electron scattering by the screened Coulomb potential as a tool to retrieve properties of the relativistic vortex beams of electrons, such as their transverse momentum and orbital angular momentum (OAM). We focus on relativistic and ultrarelativistic regimes of the electron energies of at least several MeV and higher, in which the transverse beam momentum is typically much smaller than its longitudinal momentum. Different scattering scenarios for the incident electron beam are considered. In particular, the scattering by a very wide target can be used to probe the electron transverse momentum when its values are larger than 10 keV. The scattering by a target of a width comparable to that of the incident beam allows one to obtain information about the electron OAM. Varying target sizes in the range from couple to hundreds of nanometers, one can in principle distinguish OAM values from several units of $\hbar$ up to thousands and more.

I. INTRODUCTION

Particles with a definite value of orbital angular momentum (OAM) [1–3], also dubbed *twisted* or *vortex* particles, are of considerable attention nowadays. Historically, twisted photons were the first type of such particle that inspired studies both in theoretical and experimental domains, and pioneering experiments with them took place in the 1990s. The generation of twisted electrons is a more recent research field: the first such electrons were obtained in the early 2010s [4–6]. Currently, the achievable values of OAM projection value could be as high as hundreds [7] and even thousands [8,9] of units in terms of $\hbar$. Applications of twisted electrons include such spheres as ionization by twisted electrons [10–12] and interaction of twisted electrons with matter [13,14].

Keeping up with the experiment, quantitative theoretical studies of the scattering processes with twisted electrons are in development. Let us briefly review several works. Scattering of twisted electrons by single potential atomic targets and infinitely wide (*macroscopic*) targets were considered in [15,16] in nonrelativistic and moderately relativistic regimes (electron kinetic energy up to 1 MeV). A more sophisticated approach to twisted states consists in treating them as spatially localized wave packets. Scattering of an "ordinary" Gaussian packet by a single atom, macroscopic or a localized finite-size (*mesoscopic*) targets was given in [17]. Generalizations for the case of twisted particles in nonrelativistic regime could be found in [18–20]. Here we shall consider the scattering processes with relativistic energies for a single-atom, macroscopic, and mesoscopic targets.

In this work, we revisit the topic of using electron scattering by an atomic potential as a tool for analyzing properties of the relativistic Bessel beams of electrons. It is argued in [15] that the case of scattering by a single atom is rather informative on the features of the incident twisted particle, and it is even possible to retrieve the value of the OAM projection, while, in contrast, scattering by a macroscopic target is less sensitive: transverse momentum could be deduced but not the OAM value. At the same time, calculations with a single-atom target are not straightforwardly applicable in a real experiment.

To have both a realistic and OAM sensitive scenario, we suggest taking a finite-size target, the *mesoscopic* target, following the example of [18]. We find an amplitude for the scattering off a mesoscopic target and compare it to the one off a macroscopic target. As the mesoscopic target continues naturally both into the single-atom and macroscopic scenarios, it provides a signature criterion to mark the transition between these two scenarios. We find that the transition takes place at different target sizes depending on the OAM of the incident twisted electron, and develop an idea that this can be used to retrieve the value of OAM in the experiment. Having in mind the possibilities of generating relativistic twisted electrons at particle accelerators [21–23], we pay specific attention to the ultrarelativistic energies, starting from several MeV and higher. For such energies the usual methods of analyzing the twisted electron beams used in electron microscopy, in which the typical electron energies are of order of several keVs, are hardly applicable, and that makes the proposed method of detecting OAM promising for analyzing relativistic electron beams.

In Sec. II we review the basics of Mott scattering, the modifications needed for the study of twisted electron scattering, and the technical realizations of the three aforementioned target kinds. After these introductory steps, we find scattering amplitudes for all three scenarios in Sec. III. The results acquired are analyzed in Sec. IV and, finally, the summary is presented in Sec. V. Throughout the paper we put $\hbar = c = 1$ and use Gaussian convention for the electric charge: $\alpha_0 = e^2 = 1/137$.

---

*vladislav.ivanov@metalab.ifmo.ru

II. THEORETICAL PRELIMINARIES

A. Plane-wave Mott scattering

The Mott scattering description is given in many classical textbooks [24,25]. The corresponding scattering amplitude can be written as

$$f_{\lambda,\lambda'}(\mathbf{p}, \mathbf{p}') = -\int \psi^{\dagger}_{\mathbf{p}'\lambda'}(\mathbf{r})\mathcal{V}(\mathbf{r})\psi_{\mathbf{p}\lambda}(\mathbf{r})d^3r, \qquad (1)$$

$$S_{fi} = i2\pi\delta(\varepsilon - \varepsilon')f_{\lambda,\lambda'}(\mathbf{p}, \mathbf{p}'), \qquad (2)$$

where

$$\psi_{\mathbf{p}\lambda} = \frac{1}{\sqrt{2\varepsilon V}}u_{\mathbf{p}\lambda}e^{i\mathbf{p}\mathbf{r}}, \quad \psi_{\mathbf{p}'\lambda'} = \frac{1}{\sqrt{2\varepsilon'V}}u_{\mathbf{p}'\lambda'}e^{i\mathbf{p}'\mathbf{r}} \qquad (3)$$

are the plane-wave wave functions of free electrons with incident (final) momentum, energy, and helicity $\mathbf{p}$, $\varepsilon = \sqrt{\mathbf{p}^2 + m_e^2}$ and λ ($\mathbf{p}'$, ε' and λ') and $\mathcal{V}(\mathbf{r})$ is the scattering potential, m_e is the electron mass. The Dirac bispinors $u_{\mathbf{p}\lambda}$ can be expressed as

$$u_{\mathbf{p}\lambda} = \begin{pmatrix} \sqrt{\varepsilon + m_e}w^{\lambda}(\mathbf{n}) \\ 2\lambda\sqrt{\varepsilon - m_e}w^{\lambda}(\mathbf{n}) \end{pmatrix}, \qquad (4)$$

where the spinors $w^{\lambda}(\mathbf{n})$ are the eigenfunctions of the helicity operator and $\mathbf{n} = (\sin\theta\cos\varphi, \sin\theta\sin\varphi, \cos\theta)$ is a unit vector along $\mathbf{p}$:

$$\Lambda(\mathbf{n})w^{\lambda}(\mathbf{n}) \equiv \frac{\hat{\sigma}\mathbf{n}}{2}w^{\lambda}(\mathbf{n}) = \lambda w^{\lambda}(\mathbf{n}). \qquad (5)$$

Let us choose the axes so that the incident electron propagates along the z direction. For a spinor w^{λ} along the z direction, the relation above becomes

$$\frac{\hat{\sigma}_z}{2}w^{\sigma}(\mathbf{e}_z) = \sigma w^{\sigma}(\mathbf{e}_z). \qquad (6)$$

In this case, this spinor has a simple form for the up and down spins

$$w^{1/2}(\mathbf{e}_z) = \begin{pmatrix} 1 \\ 0 \end{pmatrix}, \quad w^{-1/2}(\mathbf{e}_z) = \begin{pmatrix} 0 \\ 1 \end{pmatrix}. \qquad (7)$$

There is a standard approach that simplifies further calculation of the twisted particle amplitudes, representing electron spinors using the Wigner D functions $D^{1/2}_{\sigma\lambda}(\varphi, \theta, 0)$ [26]

$$w^{\lambda}(\mathbf{n}) = \sum_{\sigma=\pm 1/2} D^{1/2}_{\sigma\lambda}(\varphi, \theta, 0)w^{\sigma}(\mathbf{e}_z)$$
$$= \sum_{\sigma=\pm 1/2} e^{-i\sigma\varphi}d^{1/2}_{\sigma\lambda}(\theta)w^{\sigma}(\mathbf{e}_z), \qquad (8)$$

where $d^{1/2}_{\sigma\lambda}(\theta) = \delta_{\sigma,\lambda}\cos(\theta/2) - 2\sigma\delta_{\sigma,-\lambda}\sin(\theta/2)$. The bispinor $u_{\mathbf{p}\lambda}$ of the incident electron can then be expressed in the following way [22]:

$$u_{\mathbf{p}\lambda} = \sum_{\sigma=\pm 1/2} e^{-i\sigma\varphi}d^{1/2}_{\sigma\lambda}(\theta)u_{p_z\sigma}. \qquad (9)$$

Turning to $\mathcal{V}(\mathbf{r})$, the Coulomb potential is used for the conventional Mott scattering, but a more accurate result can be obtained using a screened Coulomb potential [27]

$$\mathcal{V}(\mathbf{r}) = -\frac{Ze^2}{r}e^{-\mu r}, \qquad (10)$$

where Z is a charge of the nucleus, e is an electron charge, and μ is a parameter of screening, which is set to be equal to $2m_e\alpha_0 = 2/a_0$, where a_0 is the Bohr radius in the case of hydrogen [15]. After integrating (1) with the potential (10) we find

$$f_{\lambda,\lambda'}(\mathbf{p}, \mathbf{p}') = 4\pi\frac{Ze^2}{\mathbf{q}^2 + \mu^2}u^{\dagger}_{\mathbf{p}'\lambda'}u_{\mathbf{p}\lambda}$$
$$= 4\pi\frac{2Ze^2}{\mathbf{q}^2 + \mu^2}(\varepsilon\delta_{\lambda\lambda'} + m_e\delta_{\lambda,-\lambda'})$$
$$\times \sum_{\sigma=\pm 1/2} e^{i\sigma(\varphi'-\varphi)}d^{1/2}_{\sigma\lambda}(\theta)d^{1/2}_{\sigma\lambda'}(\theta'), \qquad (11)$$

where the primed angles are of the final electron momentum. Here, for elastic scattering we have (Θ is an angle between momentum vectors)

$$\mathbf{q}^2 = (\mathbf{p} - \mathbf{p}')^2 = 2|\mathbf{p}|^2(1 - \cos\Theta)$$
$$= 2|\mathbf{p}|^2[1 - \cos\theta\cos\theta' - \sin\theta\sin\theta'\cos(\varphi-\varphi')]. \qquad (12)$$

In accordance with [15,25] the resulting cross section is

$$\frac{d\sigma}{d\Omega} = \frac{|\mathbf{p}|}{\varepsilon j_{in}}\frac{1}{16\pi^2}|f_{\lambda,\lambda'}(\mathbf{p}, \mathbf{p}')|^2, \qquad (13)$$

where j_{in} is a projection on the propagation direction of the incident particle current

$$j^{\mu} = \bar{\psi}\gamma^{\mu}\psi, \qquad (14)$$

and γ^{μ} are Dirac matrices. With the plane-wave expression (3) for the incident electron substituted into the definition (14), the identity $\bar{u}_{\mathbf{p}\lambda}\gamma^{\mu}u_{\mathbf{p}\lambda} = 2p^{\mu}$, and the incident wave propagating along z the z projection of the current is simplified to $j_z = \frac{1}{2\varepsilon}2p_z = \frac{|\mathbf{p}|}{\varepsilon}$. Then, for the cross section of the plane-wave scattering, we find

$$\left(\frac{d\sigma}{d\Omega}\right)^{(PW)} = \frac{1}{16\pi^2}|f_{\lambda,\lambda'}(\mathbf{p}, \mathbf{p}')|^2$$
$$= \frac{4Z^2e^4}{(\mathbf{q}^2 + \mu^2)^2}(\varepsilon^2\delta_{\lambda\lambda'} + m_e^2\delta_{\lambda,-\lambda'})$$
$$\times \left|\sum_{\sigma=\pm 1/2} e^{i\sigma(\varphi'-\varphi)}d^{1/2}_{\sigma\lambda}(\theta)d^{1/2}_{\sigma\lambda'}(\theta')\right|^2. \qquad (15)$$

This cross section would be useful as a reference in the following discussion.

B. Bessel twisted electrons

A twisted electron moving along the z direction is characterized by the value of the total angular momentum (TAM) operator J_z, i.e., it has a defined value of $m = 0, \pm 1, \pm 2, \ldots$. The corresponding wave function, the so-called *Bessel beam*, can be written in the following way [15]:

$$\psi_{\kappa m p_z\lambda}(\mathbf{r}) = \int \frac{d^2p_{\perp}}{(2\pi)^2}a_{\kappa m}(\mathbf{p}_{\perp})\psi_{\mathbf{p}\lambda}$$
$$= \sqrt{\frac{\kappa}{2\pi}}\sum_{\sigma=\pm 1/2} d^{1/2}_{\sigma\lambda}(\theta_p)u_{p_z\sigma}e^{ip_zz}J_{m-\sigma}(\kappa r), \qquad (16)$$

where $\mathbf{p}_\perp = (|\mathbf{p}_\perp| \cos\varphi_p, |\mathbf{p}_\perp| \sin\varphi_p)$ is the transverse part of the electron momentum $\mathbf{p}$ and $(\mathbf{p}_\perp, p_z)$ lay on the surface of a cone with an opening angle is $\theta_p = \arctan(\kappa/p_z)$, $J_{m-\sigma}(\kappa r)$ is the Bessel function of the first kind and

$$a_{\kappa m}(\mathbf{p}_\perp) = (-i)^m e^{im\varphi_p} \sqrt{\frac{2\pi}{\kappa}} \delta(|\mathbf{p}_\perp| - \kappa) \qquad (17)$$

is a Fourier coefficient with κ fixing the modulus of the transverse momentum. In the limit of $\kappa \to 0$ the twisted wave function (16) behaves like a plane wave $\psi_{p_z \lambda}$.

It is worth noting that a more general model for a twisted electron is the Laguerre-Gaussian (LG) beam that takes into account the beam spreading. However, since the Rayleigh length of the electron LG beam is much larger than the typical scale in our settings, the beam spreading is actually negligible. Moreover, in the experiment only several first rings of the LG beam profile contribute, therefore the Bessel beam is a good approximation of the twisted beam profile.

The amplitude for the scattering of the initial twisted electron is obtained via inserting the twisted wave function (16) into Eq. (1)

$$
\begin{aligned}
f_{\lambda,\lambda'}^{m,(TW)}(\mathbf{p}, \mathbf{p}', \mathbf{b}) &= -\int \psi_{\mathbf{p}'\lambda'}^\dagger(\mathbf{r}) \mathcal{V}(\mathbf{r}) \psi_{\kappa m p_z \lambda}(\mathbf{r}) d^3 r \\
&= \int \frac{d^2 p_\perp}{(2\pi)^2} a_{\kappa m}(\mathbf{p}_\perp) e^{-i\mathbf{p}_\perp \mathbf{b}} f_{\lambda\lambda'}(\mathbf{p}, \mathbf{p}') \\
&= (-i)^m \sqrt{\frac{2\pi}{\kappa}} \int_0^{2\pi} \frac{d\varphi_p}{2\pi} e^{im\varphi_p - i\mathbf{p}_\perp \mathbf{b}} f_{\lambda\lambda'}(\mathbf{p}, \mathbf{p}').
\end{aligned}
$$
$$(18)$$

With $f_{\lambda\lambda'}(\mathbf{p}, \mathbf{p}')$ given in Eq. (11) we obtain

$$
\begin{aligned}
f_{\lambda,\lambda'}^{m,(TW)}(\mathbf{p}, \mathbf{p}', \mathbf{b}) &= 8\pi Z e^2 i^{-m} \sqrt{\frac{\kappa}{2\pi}} (\varepsilon \delta_{\lambda\lambda'} + m_e \delta_{\lambda,-\lambda'}) e^{im\varphi'} \\
&\quad \times \sum_{\sigma=\pm 1/2} d_{\sigma\lambda}^{1/2}(\theta_p) d_{\sigma\lambda'}^{1/2}(\theta') \mathcal{I}_{m-\sigma}(\alpha, \beta, \mathbf{b}),
\end{aligned}
$$
$$(19)$$

where

$$\mathcal{I}_n(\alpha, \beta, \mathbf{b}) = \int \frac{d\phi}{2\pi} \frac{e^{in\phi - i\kappa b \cos(\phi + \varphi' - \varphi_b)}}{\alpha - \beta \cos\phi}, \qquad (20)$$

$$\alpha = 2|\mathbf{p}|^2 (1 - \cos\theta_p \cos\theta') + \mu^2, \qquad (21)$$

$$\beta = 2|\mathbf{p}|^2 \sin\theta_p \sin\theta'. \qquad (22)$$

It seems that the integral (20) could not be calculated in closed form. However, with some complex analysis and for the case of impact parameter $\mathbf{b} = 0$ we obtain the following analytical expression:

$$
\begin{aligned}
\mathcal{I}_n(\alpha, \beta, 0) &= \int \frac{d\phi}{2\pi} \frac{e^{in\phi}}{\alpha - \beta \cos\phi} \\
&= -\frac{1}{i\pi\beta} \oint_{|z| \leqslant 1} \frac{z^{|n|}}{(z - \zeta_1)(z - \zeta_2)} \qquad (23) \\
&= -\frac{2}{\beta} \frac{\zeta_2^{|n|}}{\zeta_2 - \zeta_1},
\end{aligned}
$$

where $\zeta_1 > 1$, $\zeta_2 < 1$

$$\zeta_{1,2} = \frac{\alpha}{\beta} \left(1 \pm \sqrt{1 - \frac{\beta^2}{\alpha^2}}\right). \qquad (24)$$

Equation (23) can be now expressed as

$$\mathcal{I}_n(\alpha, \beta, 0) = \frac{1}{\sqrt{\alpha^2 - \beta^2}} \left(\frac{\alpha - \sqrt{\alpha^2 - \beta^2}}{\beta}\right)^{|n|}. \qquad (25)$$

Similar results are given in [15,19].

For small θ_p, the integral (20) transforms into

$$
\begin{aligned}
\mathcal{I}_n(\alpha, 0, \mathbf{b}) &= \int \frac{d\phi}{2\pi} \frac{e^{in\phi - i\kappa b \cos(\phi + \varphi' - \varphi_b)}}{\alpha} \\
&= \frac{1}{\alpha} e^{-in(\varphi' - \varphi_b)} J_n(\kappa b). \qquad (26)
\end{aligned}
$$

We remark that for the large $\kappa b \gg 1$ the integral (20) can be evaluated approximately using the method of stationary phase [28,29]. We show how it can be done in Appendix B.

C. Distribution of atoms in the target

As was mentioned in the Introduction we shall analyze electron scattering by the targets of three types: single atom, macroscopic, and mesoscopic. Physically, such targets can be represented by a thin foil much wider than the beam size for the macroscopic or a round piece of thin foil for the mesoscopic target. To model a target we average the amplitude (19) with some distribution function $n(\mathbf{b})$:

$$F_{m,\lambda,\lambda'}(\mathbf{p}, \mathbf{p}', \mathbf{b}) = \int d^2 b \, n(\mathbf{b}) f_{\lambda,\lambda'}^{m,(TW)}(\mathbf{p}, \mathbf{p}', \mathbf{b}). \qquad (27)$$

We use the following functions for each target type

$$n^{\text{macro}}(\mathbf{b}) = \frac{1}{\pi R^2}, \qquad (28)$$

$$n^{\text{single}}(\mathbf{b}) = \delta(\mathbf{b} - \mathbf{b}_0), \qquad (29)$$

$$n^{\text{meso}}(\mathbf{b}) = \frac{1}{2\pi\sigma_b^2} e^{-\frac{1}{2}\left(\frac{\mathbf{b} - \mathbf{b}_0}{\sigma_b}\right)^2}, \qquad (30)$$

where R is an arbitrary large radius taken as an integration limit in the macroscopic scenario. In the latter two cases [Eqs. (29) and (30)] $\mathbf{b}_0$ is either a target position or a target center, while σ_b gives an effective target size. All three distributions obey the normalization condition $\int d^2 b \, n(\mathbf{b}) = 1$.

The mesoscopic distribution (30) should reduce to (28) for a large target size ($\sigma_b \to \infty$); we have

$$n^{\text{meso}}(\mathbf{b}) \approx \frac{1}{2\pi\sigma_b^2} \sim n^{\text{macro}}(\mathbf{b}). \qquad (31)$$

In the limit of small σ_b, the mesoscopic distribution is reduced to the Dirac delta.

III. SCATTERING OFF DIFFERENT TARGETS

In this section, we present the results for the scattering of a twisted electron by different targets. Results for the

single-atom and the macroscopic target are similar to those presented in [15]. Though, we are more interested in the relativistic energies of the incident electron and focus on the regime when θ_p is rather small ($p_z \gg \kappa$) or, equivalently, when the factor β of (22) is small. For instance, ultrarelativistic electrons with $\varepsilon = 100m_e$ and $\kappa \sim 10$ keV have the value of angle $\theta_p \approx 0.01°$, and therefore, $\alpha \gg \beta$. We assume, that the electron scatters on different atoms independently and obtain scattering amplitude by summing the contributions of scattering by individual potentials. This approach seems to be adequate for the beam size typically larger than the atomic scale. For the specifics of considering more tightly focused beams we refer the reader to [30]. We also provide calculations for the relativistic electron scattering by a mesoscopic target, which are complementary to those made in [18] in the nonrelativistic regime.

A. Macroscopic target

The simplest case is scattering by a macroscopic target. In this scenario, we can obtain an analytic expression for the cross section. Let us start with squaring the corresponding amplitude

$$
\left|F_{m,\lambda,\lambda'}^{(\text{macro})}(\mathbf{p}, \mathbf{p}')\right|^2 = \frac{1}{\pi R^2} \frac{2\pi}{\kappa} \int \frac{d^2\mathbf{p}_\perp}{(2\pi)^2}
$$
$$
\times |f_{\lambda\lambda'}(\mathbf{p}, \mathbf{p}')\delta(|\mathbf{p}_\perp| - \kappa)|^2, \quad (32)
$$

where we use that $\int d^2b\, e^{i(\mathbf{k}_\perp - \mathbf{p}_\perp)\mathbf{b}} = (2\pi)^2\delta(\mathbf{k}_\perp - \mathbf{p}_\perp)$. Further, one can use the following identity (see, for example, [31]):

$$
|\delta(|\mathbf{p}_\perp| - \kappa)|^2 = \frac{R}{\pi}\delta(|\mathbf{p}_\perp| - \kappa). \quad (33)
$$

Then it turns out that

$$
\left|F_{m,\lambda,\lambda'}^{(\text{macro})}(\mathbf{p}, \mathbf{p}')\right|^2 = \frac{1}{R}64Z^2e^4\left(\varepsilon^2\delta_{\lambda\lambda'} + m_e^2\delta_{\lambda,-\lambda'}\right)
$$
$$
\times \sum_{\sigma,\sigma'} d_{\sigma\lambda}^{1/2}(\theta_p)d_{\sigma\lambda'}^{1/2}(\theta')d_{\sigma'\lambda}^{1/2}(\theta_p)d_{\sigma'\lambda'}^{1/2}(\theta')
$$
$$
\times \int_0^{2\pi} \frac{d\varphi_p}{2\pi} \frac{e^{i(\sigma-\sigma')(\varphi_p-\varphi')}}{[\alpha - \beta\cos(\varphi_p - \varphi')]^2}. \quad (34)
$$

The integral in the above expression can be expressed through the integral (23)

$$
\int_0^{2\pi} \frac{d\varphi_p}{2\pi} \frac{e^{i(\sigma-\sigma')(\varphi_p-\varphi')}}{[\alpha - \beta\cos(\varphi_p - \varphi')]^2} = -\frac{\partial}{\partial\alpha}\mathcal{I}_{\sigma'-\sigma}(\alpha, \beta, 0)
$$
$$
= \frac{\alpha\delta_{\sigma,\sigma'} + \beta\delta_{\sigma,\sigma'}}{(\alpha^2 - \beta^2)^{3/2}}. \quad (35)
$$

To find the cross section we need to calculate the incident electron current j_z. In contrast to the plane-wave case, for a twisted wave function we need to average the current over the incident plane [15]

$$
j_z^{(\text{macro})} = \frac{1}{\pi R^2} \int d^2b\, \bar{\psi}_{\kappa mp_z\lambda}(\mathbf{b})\gamma^3\psi_{\kappa mp_z\lambda}(\mathbf{b})
$$

$$
= \frac{1}{2\varepsilon\pi R^2}\frac{\kappa}{2\pi} \int d^2b \sum_{\sigma,\sigma'} d_{\sigma\lambda}^{1/2}(\theta_p)d_{\sigma'\lambda}^{1/2}(\theta_p)\bar{u}_{p_z\sigma}\gamma^3 u_{p_z\sigma'} \int_0^{2\pi} \frac{d\varphi_p}{2\pi}e^{i(m-\sigma')\varphi_p - i\kappa b\cos\varphi_p} \int_0^{2\pi} \frac{d\varphi_p}{2\pi}e^{-i(m-\sigma)\varphi_p + i\kappa b\cos\varphi_p}
$$

$$
= \frac{1}{\pi R^2}\frac{p_z}{\varepsilon} \int_0^\infty db\, \kappa b J_{m-\lambda}^2(\kappa b) = \frac{p_z}{\varepsilon}\frac{1}{\pi^2 R}. \quad (36)
$$

Using Eq. (13) for the cross section, we find

$$
\left(\frac{d\sigma}{d\Omega}\right)^{(\text{macro})} = \frac{4Z^2e^4}{\cos\theta_p}\left(\varepsilon^2\delta_{\lambda\lambda'} + m_e^2\delta_{\lambda,-\lambda'}\right)\sum_{\sigma,\sigma'} d_{\sigma\lambda}^{1/2}(\theta)d_{\sigma\lambda'}^{1/2}(\theta')d_{\sigma'\lambda}^{1/2}(\theta)d_{\sigma'\lambda'}^{1/2}(\theta')\frac{\alpha\delta_{\sigma,\sigma'} + \beta\delta_{\sigma,-\sigma'}}{(\alpha^2 - \beta^2)^{3/2}}. \quad (37)
$$

Notice the factor $\sim 1/(\alpha^2 - \beta^2)$ in the expression above. It leads to the appearance of a characteristic resonance peak in the cross-section graph (see Figs. 1 and 2), its position around $\theta' \simeq \theta_p$.

Let us rewrite the plane wave expression (15) in different terms for convenience

$$
\left(\frac{d\sigma}{d\Omega}\right)^{(PW)} = \frac{4Z^2e^4}{\alpha^2}\left(\varepsilon^2\delta_{\lambda\lambda'} + m_e^2\delta_{\lambda,-\lambda'}\right)
$$
$$
\times \left|\sum_{\sigma=\pm 1/2} e^{i\sigma(\varphi'-\varphi)}d_{\sigma\lambda}^{1/2}(\theta)d_{\sigma\lambda'}^{1/2}(\theta')\right|^2. \quad (38)
$$

Then, if we go into the relativistic regime in (37) (neglecting the β terms and assuming $\cos\theta_p = 1$) we find coincidence with (38)

$$
\lim_{\theta_p\to 0}\left(\frac{d\sigma}{d\Omega}\right)^{(\text{macro})} = 4Z^2e^4\left(\varepsilon^2\delta_{\lambda\lambda'} + m_e^2\delta_{\lambda,-\lambda'}\right)
$$
$$
\times \left|\sum_{\sigma=\pm 1/2} d_{\sigma\lambda}^{1/2}(\theta_p)d_{\sigma\lambda'}^{1/2}(\theta')\right|^2 \frac{1}{\alpha^2}
$$
$$
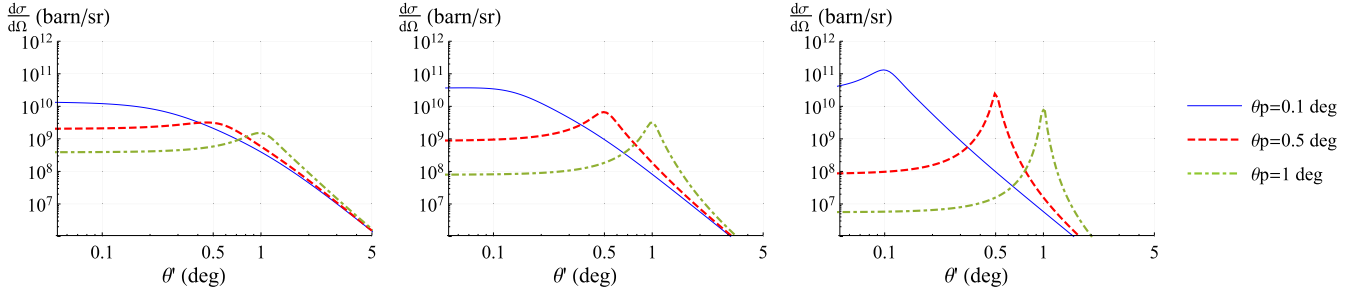= \left(\frac{d\sigma}{d\Omega}\right)^{(PW)}. \quad (39)
$$

FIG. 1. The cross section for a macrospic iron target and relativistic electron energies. Left panel: $\varepsilon = 2m_e$, blue solid $\theta_p = 0.1°$ ($\kappa = 1.5$ keV), dashed red $\theta_p = 0.5°$ ($\kappa = 7.7$ keV), dot dashed green $\theta_p = 1°$ ($\kappa = 15$ keV). Middle panel: $\varepsilon = 5m_e$, blue solid $\theta_p = 0.1°$ ($\kappa = 4.4$ keV), dashed red $\theta_p = 0.5°$ ($\kappa = 21.9$ keV), dot dashed green $\theta_p = 1°$ ($\kappa = 43$ keV). Right panel: $\varepsilon = 20m_e$, blue solid $\theta_p = 0.1°$ ($\kappa = 17.8$ keV), dashed red $\theta_p = 0.5°$ ($\kappa = 89$ keV), dot dashed green $\theta_p = 1°$ ($\kappa = 178$ keV).

This expression is approximately valid for the values of $\theta_p \lesssim 5$ deg, but near the resonance the Taylor series converges much slower. However, for small $\kappa \lesssim 10$ keV the resonance is barely distinguishable (see Fig. 1). Hence, the macroscopic
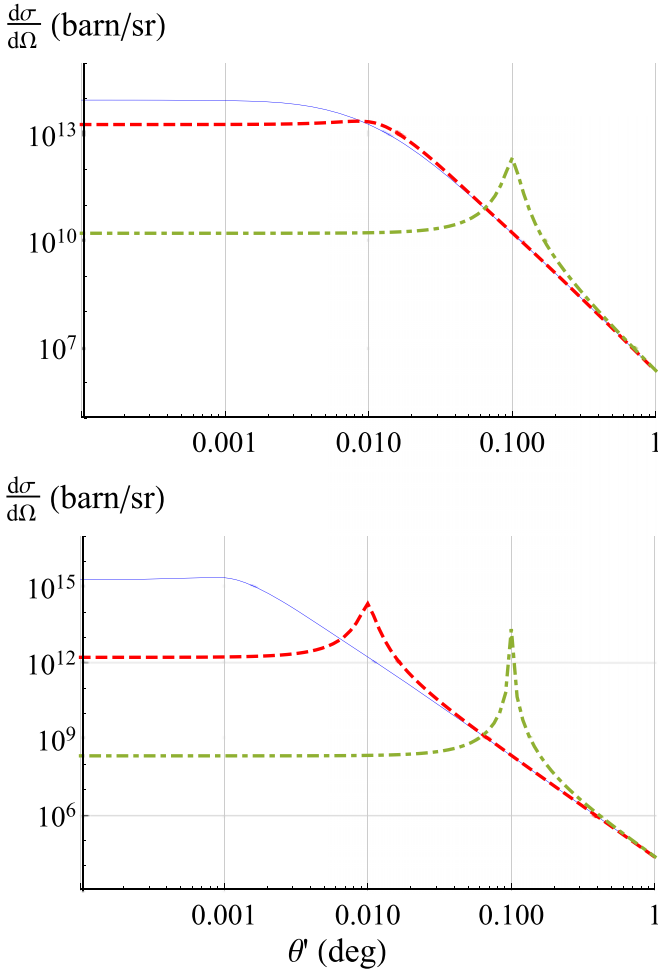

FIG. 2. The cross section for a macrospic golden target and ultrarelativistic electron energies. Top panel: $\varepsilon = 100m_e$, blue solid $\theta_p = 0.001°$ ($\kappa = 0.89$ keV), dashed red $\theta_p = 0.01°$ ($\kappa = 8.9$ keV), dot dashed green $\theta_p = 0.1°$ ($\kappa = 89$ keV). Bottom panel: $\varepsilon = 1000m_e$, blue solid $\theta_p = 0.001°$ ($\kappa = 8.9$ keV), dashed red $\theta_p = 0.01°$ ($\kappa = 89$ keV), dot dashed green $\theta_p = 0.1°$ ($\kappa = 891$ keV).

cross section is well approximated by the plane-wave one for $\theta_p \lesssim 5$ deg when we are not interested in scattering angles near the resonance or when κ is small.

In the discussion above, we use the screened Coulomb potential (10). However, as was proposed in [15], we can use an alternative form of the potential: an analytical fit to the self-consistent Dirac-Hartree-Fock-Slater data [32]. It is assumed to provide a more realistic description of atom-electron collisions. Such a potential would read

$$\mathcal{V}_{at}(r) = -\frac{Ze^2}{r} \sum_{i=1}^{3} A_i e^{-\mu_i r}, \qquad (40)$$

where the coefficients A_i and μ_i depend on the atomic number and are given in [32], $A_1 + A_2 + A_3 = 1$. See the coefficients for iron and gold in Table I.

We can implement this new potential into our calculations. For scattering by a macroscopic target, the result for the cross section was obtained in [15]. Repeating all the previous steps we find

$$\left(\frac{d\sigma}{d\Omega}\right)_{at}^{(\text{macro})} = \frac{4Z^2 e^4}{\cos\theta_p}\left(\varepsilon^2 \delta_{\lambda\lambda'} + m_e^2 \delta_{\lambda,-\lambda'}\right)$$
$$\times \sum_{\sigma,\sigma'} d_{\sigma\lambda}^{1/2}(\theta) d_{\sigma\lambda'}^{1/2}(\theta') d_{\sigma'\lambda}^{1/2}(\theta) d_{\sigma'\lambda'}^{1/2}(\theta') \qquad (41)$$
$$\times \sum_{i,k=1}^{3} A_i A_k \mathcal{I}_{\sigma-\sigma'}^{at}(\alpha_i, \alpha_k, \beta),$$

$$\mathcal{I}_n^{at}(\alpha_i, \alpha_k, \beta) = \begin{cases} \dfrac{\alpha_i \delta_{\sigma,\sigma'} + \beta \delta_{\sigma,\sigma'}}{(\alpha_i^2 - \beta^2)^{3/2}}, & \text{if } i = k, \\[2ex] \dfrac{\mathcal{I}_n(\alpha_i, \beta, 0) - \mathcal{I}_n(\alpha_k, \beta, 0)}{\alpha_k - \alpha_i}, & \text{if } i \neq k. \end{cases}$$
$$(42)$$

TABLE I. Parameters of atomic potential (40) for some elements [15,32].

Elem.	A_1	A_2	$\mu_1/(m_e\alpha_0)$	$\mu_2/(m_e\alpha_0)$	$\mu_3/(m_e\alpha_0)$
Fe(26)	0.0512	0.6995	31.825	3.7716	1.1606
Cu(29)	0.0771	0.7951	25.326	3.3928	1.1426
Ag(47)	0.2562	0.6505	15.588	2.7412	1.1408
Au(79)	0.2289	0.6114	22.864	3.6914	1.4886

Since $\mathcal{I}_n(\alpha, \beta, 0)$ is proportional to $1/\sqrt{\alpha^2 - \beta^2}$, so is the function $\mathcal{I}^{at}_{\sigma-\sigma'}(\alpha_i, \alpha_k, \beta)$. Therefore, the cross section (41) with the modified potential manifests the same resonance as Eq. (37).

For small θ_p, the cross section (41) is reduced to

$$\lim_{\theta_p \to 0} \left(\frac{d\sigma}{d\Omega} \right)^{(\text{macro})}_{at} = 4Z^2 e^4 \left(\varepsilon^2 \delta_{\lambda\lambda'} + m_e^2 \delta_{\lambda,-\lambda'} \right)$$
$$\times \left(\sum_{i=1}^3 \frac{A_i}{\alpha_i} \right)^2 \left| \sum_{\sigma=\pm 1/2} d^{1/2}_{\sigma\lambda}(\theta_p) d^{1/2}_{\sigma\lambda'}(\theta') \right|^2.$$
(43)

Shall we decide to deal with a detector that is insensitive to the electron polarization, the sum of the cross section over final polarizations λ' is necessary.

B. Single-atom target

Now we shall analyze the scattering by a single-atom potential. The distribution function for the scattering by a single atom is given by (29) and the squared scattering amplitude then reads

$$\left| F^{(\text{single})}_{m,\lambda,\lambda'}(\mathbf{p}, \mathbf{p}') \right|^2$$
$$= |F(\mathbf{p}, \mathbf{p}', \mathbf{b}_0)|^2$$
$$= 32\pi Z^2 e^4 \kappa \left(\varepsilon^2 \delta_{\lambda\lambda'} + m_e^2 \delta_{\lambda,-\lambda'} \right)$$
$$\times \left| \sum_{\sigma=\pm 1/2} d^{1/2}_{\sigma\lambda}(\theta_p) d^{1/2}_{\sigma\lambda'}(\theta') \mathcal{I}_{m-\sigma}(\alpha, \beta, \mathbf{b}_0) \right|^2. \quad (44)$$

In contrast to the previous cases, obtaining an analytic result here is obstructed due to an ambiguity in defining the cross section. The problem is that the incident current j_z goes to zero for some values of the impact parameter since $j_z \sim J^2_{m-\lambda}(\kappa b_0)$, and hence the usage of (13) is compromised (see also a discussion on this issue given in [15]). To overcome this obstacle, we go instead to the consideration of the number of scattering events, following the lead of the authors of [18,33]

$$d\nu \equiv N_e |S_{fi}|^2 \frac{V d^3 p'}{(2\pi)^3}, \quad (45)$$

where N_e is a number of incident electrons. Then we acquire a relation similar to the cross-section formula

$$\left(\frac{d\nu}{d\Omega} \right)^{(\text{single})} = \frac{N_e}{16\pi^2} \frac{|\mathbf{p}|}{\varepsilon} \left| F^{(\text{single})}_{m,\lambda,\lambda'}(\mathbf{p}, \mathbf{p}') \right|^2. \quad (46)$$

The *luminosity* [18,34] then reads

$$L^{(TW)} = N_e \frac{\kappa}{2\pi} \frac{|\mathbf{p}|}{\varepsilon} \frac{\pi T}{RL_z} = N_e \frac{\kappa}{2\pi} \frac{\pi |\mathbf{p}|}{Rv\varepsilon} = \frac{N_e}{\cos\theta_p} \frac{\kappa}{2\pi} \frac{\pi}{R},$$
(47)

where we write explicitly the normalization factor and use $L_z = vT$, where v is a velocity of the incident electron. The

large factor R does not cancel here because in our setup the wave beam is not regularized (compare with [18]). However, it can be approximately identified with the beam size, see Appendix A. Moreover, as we shall see further, in the physically meaningful results this factor will eventually cancel out.

Substituting the single-atom scattering amplitude (44) into Eq. (46) we find

$$\left(\frac{d\nu}{d\Omega} \right)^{(\text{single})} = \frac{N_e}{\cos\theta_p} \frac{\kappa}{R} 2Z^2 e^4 \left(\varepsilon^2 \delta_{\lambda\lambda'} + m_e^2 \delta_{\lambda,-\lambda'} \right)$$
$$\times \left| \sum_{\sigma=\pm 1/2} d^{1/2}_{\sigma\lambda}(\theta_p) d^{1/2}_{\sigma\lambda'}(\theta') \mathcal{I}_{m-\sigma}(\alpha, \beta, \mathbf{b}_0) \right|^2. \quad (48)$$

For small θ_p this formula is reduced to

$$\left(\frac{d\nu}{d\Omega} \right)^{(\text{single})} = N_e \frac{\kappa}{2R} J^2_{m-\lambda}(\kappa b_0) \left(\frac{d\sigma}{d\Omega} \right)^{(\text{PW})}$$
$$= L^{(TW)} J^2_{m-\lambda}(\kappa b_0) \left(\frac{d\sigma}{d\Omega} \right)^{(\text{PW})}. \quad (49)$$

Note that for $\kappa = 0$ this quantity equals to the plane wave cross-section times the luminosity factor. In principle, we can backtrack this relation and define the twisted cross section for the scattering by a single-atom target the following way [18]:

$$\left(\frac{d\sigma}{d\Omega} \right)^{(\text{single})} \equiv \frac{1}{L^{(TW)}} \left(\frac{d\nu}{d\Omega} \right)^{(\text{single})}$$
$$= J^2_{m-\lambda}(\kappa b_0) \left(\frac{d\sigma}{d\Omega} \right)^{(\text{PW})}. \quad (50)$$

C. Mesoscopic target

It was shown in [15] that with a macroscopic target, the sensitivity to the OAM of the incoming twisted electron is lost. However, a single-atom target is not the simplest experimentally realizable option, though a possible one (see, for example, [35]). Moreover, a trapped atom target has a spatial probability distribution of some considerable width (typically hundreds of nanometers) and therefore is realistically described as a wave packet and the method of the previous subsection is not applicable. A finite-size mesoscopic target appears as a more experimentally viable option, is easier to prepare (with respect to a single-atom one), and could still lead to experimental differentiation of the OAM values. We shall model such a target by a Gaussian distribution (30)

$$\left| F^{(\text{meso})}_{m,\lambda,\lambda'}(\mathbf{p}, \mathbf{p}', \mathbf{b}_0) \right|^2 = \int d^2 b \, |F(\mathbf{p}, \mathbf{p}', \mathbf{b})|^2 \frac{e^{-\frac{1}{2} \left(\frac{\mathbf{b} - \mathbf{b}_0}{\sigma_b} \right)^2}}{2\pi\sigma_b^2}. \quad (51)$$

The calculations of the amplitude and the number of events are similar to the ones in the previous section and can be found in Appendix C.

Number of events in the limit of small β and $\mathbf{b}_0 = 0$ equals

$$
\begin{aligned}
\left(\frac{d\nu}{d\Omega}\right)^{(\text{meso})} &= e^{-\sigma_b^2\kappa^2}\frac{2Z^2e^4}{\alpha^2}I_{m-\lambda}\left(\sigma_b^2\kappa^2\right) \\
&\quad \times \frac{\kappa}{R}\frac{N_e}{\cos\theta_p}\left[\varepsilon^2\cos\left(\theta'/2\right)\delta_{\lambda,\lambda'}\right. \\
&\quad \left. + m_e^2\sin\left(\theta'/2\right)\delta_{\lambda,-\lambda'}\right] \\
&= e^{-\sigma_b^2\kappa^2}I_{m-\lambda}\left(\sigma_b^2\kappa^2\right)L^{(TW)}\left(\frac{d\sigma}{d\Omega}\right)^{(PW)}, \quad (52)
\end{aligned}
$$

where $I_{m-\lambda}(\sigma_b^2\kappa^2)$ is the modified Bessel function of first kind.

For a point-like target, $\sigma_b = 0$, the modified Bessel function turns out to be equal to

$$
I_{m-\lambda}(0) = \delta_{m-\lambda,0}. \quad (53)
$$

Then, we have the following expression for the number of events:

$$
\begin{aligned}
\left(\frac{d\nu}{d\Omega}\right)^{(\text{meso})} &\to \delta_{m-\lambda,0}L^{(TW)}\left(\frac{d\sigma}{d\Omega}\right)^{(PW)} \\
&= \left(\frac{d\nu}{d\Omega}\right)^{(\text{single})}(\mathbf{b}=0). \quad (54)
\end{aligned}
$$

For a large target with $\sigma_b \sim R \to \infty$, the modified Bessel function has the following limit:

$$
I_{m-\lambda}\left(\sigma_b^2\kappa^2\right) \to \frac{e^{\sigma_b^2\kappa^2}}{\sqrt{2\pi}\,\sigma_b\kappa}. \quad (55)
$$

Then for the number of events we have

$$
\left(\frac{d\nu}{d\Omega}\right)^{(\text{meso})} = \frac{1}{\sqrt{2\pi}\,\sigma_b\kappa}\frac{\kappa}{2R}\frac{N_e}{\cos\theta_p}\left(\frac{d\sigma}{d\Omega}\right)^{(PW)}. \quad (56)
$$

For the realistic atomic potential (40) and small β, we find

$$
\begin{aligned}
\left(\frac{d\nu}{d\Omega}\right)^{(\text{meso})} &= e^{-\sigma_b^2\kappa^2}2Z^2e^4\left(\sum_{i=1}^{3}\frac{A_i}{\alpha_i}\right)^2 I_{m-\lambda}\left(\sigma_b^2\kappa^2\right) \\
&\quad \times \frac{\kappa}{R}\frac{N_e}{\cos\theta_p}\left[\varepsilon^2\cos\left(\theta'/2\right)\delta_{\lambda,\lambda'}\right. \\
&\quad \left. + m_e^2\sin\left(\theta'/2\right)\delta_{\lambda,-\lambda'}\right]. \quad (57)
\end{aligned}
$$

To compare the scattering by the mesoscopic target to the macroscopic scenario, we need to introduce $d\nu/d\Omega$ in the latter case

$$
\left(\frac{d\nu}{d\Omega}\right)^{(\text{macro})} = \frac{N_e}{16\pi^2}\frac{|\mathbf{p}|}{\varepsilon}\left|F_{m,\lambda,\lambda'}^{(\text{macro})}(\mathbf{p},\mathbf{p}')\right|^2. \quad (58)
$$

In the limit of small θ_p,

$$
\begin{aligned}
\left(\frac{d\nu}{d\Omega}\right)^{(\text{macro})} &= \frac{\pi}{R}\frac{N_e}{\cos\theta_p}\frac{1}{\pi^2 R}\left(\frac{d\sigma}{d\Omega}\right)^{(PW)} \\
&= \frac{2}{\pi R\kappa}\frac{\kappa}{2R}\frac{N_e}{\cos\theta_p}\left(\frac{d\sigma}{d\Omega}\right)^{(PW)}. \quad (59)
\end{aligned}
$$

If we assume that $R = 2\sqrt{2/\pi}\,\sigma_b$, then (59) is equal to (56). This means that in the limit of the large target the scattering

of a twisted electron by a mesoscopic target becomes similar to the scattering by a macroscopic one in accordance with our mundane intuition. To "measure" this effect for any given target size σ_b we define the following ratio:

$$
\mathcal{R}_{m-\lambda}(\sigma_b,\kappa) \equiv \left(\frac{d\nu}{d\Omega}\right)^{(\text{meso})}\Big/\left(\frac{d\nu}{d\Omega}\right)^{(\text{macro})}. \quad (60)
$$

In the limit of small β and for $\mathbf{b}_0 = 0$ (typical for relativistic regime) we have

$$
\mathcal{R}_{m-\lambda}(\sigma_b,\kappa) = \sqrt{2\pi}\,\sigma_b\kappa\, e^{-\sigma_b^2\kappa^2}I_{m-\lambda}\left(\sigma_b^2\kappa^2\right). \quad (61)
$$

Here we use the amplitudes for the potential (10), but this relation holds also for the realistic potential (40) since factors $\sum A_i/\alpha_i$ cancel in the considered limit.

Our idea behind the introduction of the function $\mathcal{R}$ is that it would manifest how the scattering result varies with changing the target size from a point-like atom to an infinitely large target. Several examples are given in Fig. 3. Moreover, with this ratio we can explore the process sensitivity to the incident electron OAM value.

So far we used the Gaussian distribution (30) to model the mesoscopic target. Alternatively, we can use the uniform distribution on a finite interval

$$
\left|F_{m,\lambda,\lambda'}^{(\text{meso})}(\mathbf{p},\mathbf{p}',0)\right|^2 = \int_{S_b}d^2b\,|F(\mathbf{p},\mathbf{p}',\mathbf{b})|^2\frac{1}{\pi R_b^2}, \quad (62)
$$

where R_b is a radius of the circular target and S_b is its area. In terms of the number of events, we have the following:

$$
\left(\frac{d\nu}{d\Omega}\right)^{(\text{meso})} = \int_{S_b}d^2b\,\frac{1}{\pi R_b^2}\left(\frac{d\nu}{d\Omega}\right)^{(\text{single})}. \quad (63)
$$

Equation (49) can be used for the single-atom target in the limit $\beta \to 0$, then for (63) we find

$$
\left(\frac{d\nu}{d\Omega}\right)^{(\text{meso})} = \int_{S_b}d^2b\,\frac{1}{\pi R_b^2}J_{m-\lambda}^2(\kappa b)L^{(TW)}\left(\frac{d\sigma}{d\Omega}\right)^{(PW)}. \quad (64)
$$

This integral can be evaluated numerically and the results are shown in Fig. 4, where we plot $(d\nu/d\Omega)/\mathcal{L}$, with $\mathcal{L} \equiv L^{(TW)} \times (d\sigma/d\Omega)^{(PW)}$, for the Gaussian mesoscopic (52), the uniform mesoscopic, and the macroscopic targets, all in the relativistic limit of small β.

IV. RESULTS

First, we would like to numerically motivate an approximation used in the previous section, i.e., that, for the relativistic regime, one can assume the transverse momentum κ to be small relative to total linear momentum of the incident electron. We start with determining the opening angle θ_p value from the typical scale of the incident wave beam. In our framework we can define the characteristic beam width r_{beam} either from the half-width radius of the squared wave function
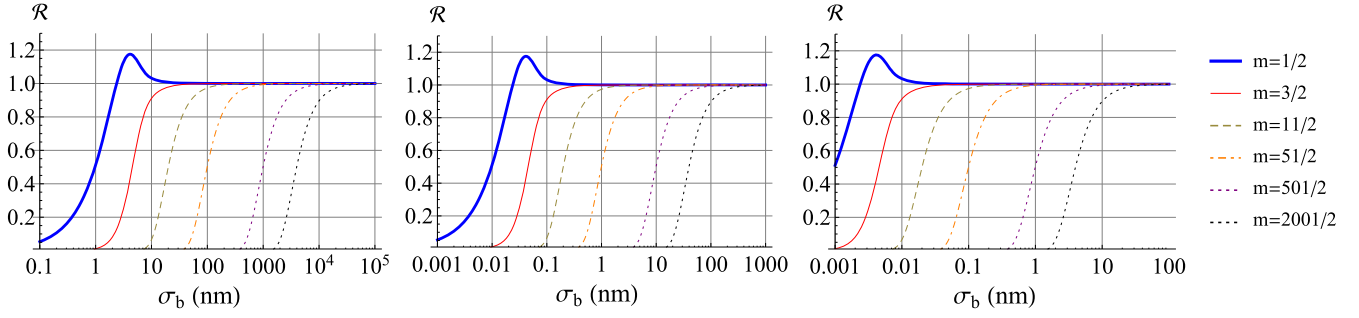
FIG. 3. The ratio of the numbers of events $\mathcal{R}_{m-\lambda} = (d\nu/d\Omega)^{(\text{meso})}/(d\nu/d\Omega)^{(\text{macro})}$ from Eq. (61) for different TAM projections m. Parameters: $\varepsilon = 5 \, m_e$, $\lambda = 1/2$. Left panel: $\theta_p = 0.001$ deg, $\kappa = 44$ eV; middle panel: $\theta_p = 0.1$ deg, $\kappa = 4.4$ keV; right panel: $\theta_p = 1$ deg, $\kappa = 44$ keV.

for the zero-order beam or from matching the first maximum for the higher-order modes [first maximum of $J_n(z)$ is situated
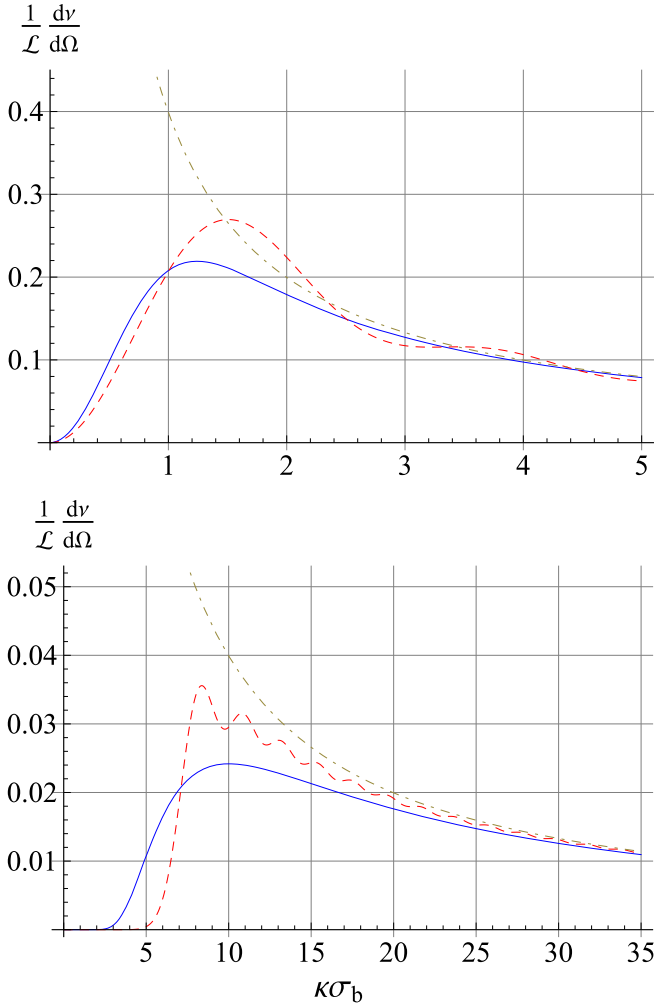

FIG. 4. Comparison of the number of scattering events functions for the Gaussian mesoscopic (blue solid line), the uniform mesoscopic (red dashed line), and the macroscopic (green dot dashed line) targets. Parameters: $m - \lambda = 1$ (top panel) and $m - \lambda = 10$ (bottom panel), the uniform target radius $R_b = 2\sqrt{2/\pi}\sigma_b$, see before Eq. (60).

at $z \approx n$]

$$\kappa \approx \begin{cases} 1/r_{\text{beam}}, & \text{if } m - \lambda = 0, \\ \dfrac{m - \lambda}{r_{\text{beam}}}, & \text{otherwise.} \end{cases} \quad (65)$$

For an angle between the total linear momentum and the propagation axis that gives

$$\theta_p \approx \begin{cases} \arcsin\left(\dfrac{1}{r_{\text{beam}}\sqrt{\varepsilon^2 - m_e^2}}\right), & \text{if } m - \lambda = 0, \\ \arcsin\left(\dfrac{m - \lambda}{r_{\text{beam}}\sqrt{\varepsilon^2 - m_e^2}}\right), & \text{otherwise.} \end{cases} \quad (66)$$

In Table II we assemble our estimations for κ and θ_p for various widths r_{beam} after setting $\varepsilon = 2m_e$. Such beam widths are currently obtainable for the electron vortices [36,37]. We can see that small values of θ_p ($\lesssim 1$ deg) are typical for a rather wide range of beam parameters, thus justifying the approximation made in the previous section. In the case of larger incident energy ε and other parameters fixed, θ_p tends to become even smaller, as $\theta_p \propto \varepsilon^{-1}$ for large ε. For example, for $\varepsilon = 10m_e$, $m - \lambda = 1$, and $r_{\text{beam}} = 1$ nm we have $\theta_p = 1.15 \times 10^{-3}$ deg. We remark, though, that large θ_p values are not uncommon for some energies, see, for instance, the analysis of [15] for the nonrelativistic incident electron.

Let us now go back to the figures that were introduced earlier in the paper. In Fig. 1 the results for differential cross section for incident relativistic ($\varepsilon/m_e = 2, 5, 20$) twisted electron scattered by a macroscopic iron target are presented. The position of the peak corresponds to the value of the opening angle for the twisted electron $\theta' = \theta_p$; determining θ' from the scattering and knowing the electron energy from beforehand one can easily calculate the transverse momentum κ. However, this peak is distinguishable only for values of $\kappa \gtrsim 10$ keV. This sets a threshold for measuring the κ with the described method. The value of 10 keV comes from the screening parameter μ, which is approximately equal to the inverse Bohr radius, being the natural scale of the problem. In Fig. 2 we take a golden macroscopic target and electrons with ultrarelativistic energies ($\varepsilon/m_e = 100, 1000$) and observe a similar picture. In fact, the scattering picture does not alter substantially with the change of the element: for higher values of Z the cross section increases in general, but the peak

TABLE II. The values of the transverse momentum κ (eV) and the angle θ_p (deg) with $\varepsilon = 2m_e$ and different wave beam width.

	κ (eV) [θ_p (deg)]			
$m - \lambda$	$r_{beam} = 1$ Å	$r_{beam} = 1$ nm	$r_{beam} = 10$ nm	$r_{beam} = 1\mu$m
1	2×10^3 (1.3×10^{-1})	2×10^2 (1.3×10^{-2})	2×10 (1.3×10^{-3})	2×10^{-1} (1.3×10^{-5})
5	1×10^4 (6.6×10^{-1})	1×10^3 (6.6×10^{-2})	1×10^2 (6.6×10^{-3})	1 (6.6×10^{-5})
10	2×10^4 (1.3)	2×10^3 (1.3×10^{-1})	2×10^2 (1.3×10^{-2})	2 (1.3×10^{-4})
100	2×10^5 (1.3×10)	2×10^4 (1.3)	2×10^3 (1.3×10^{-1})	2×10 (1.3×10^{-3})
1000	–	2×10^5 (1.3×10)	2×10^4 (1.3)	2×10^2 (1.3×10^{-3})

becomes less pronounced, as can be seen in Fig. 5 for iron, copper, silver, and gold targets.

The values of $\kappa \gg 10$ keV in Figs. 1 and 2 are hardly achievable in the experiment and are presented here mainly to illustrate the tendencies of the cross sections. Furthermore, for $\kappa \gg 10$ keV the width of the beam may became smaller than the size of an atom and that can make our target model inapplicable. However, the increase of κ can be compensated for by the increase of the OAM value, see (65).

The scattering by a macroscopic target is at a disadvantage because it cannot provide information about the electron OAM, whereas the scattering by a single-atom target or by a mesoscopic target can. We reproduce here the formula for the single-atom scattering amplitude (48) and find its approximation for small angle θ_p (49). In the relativistic regime, the amplitude of this process can be found analytically.

For the scattering by a mesoscopic target, we obtain an analytical solution for the amplitude when the target is centered ($\mathbf{b}_0 = 0$) and the angle θ_p is small. This approach was studied in [18] for the nonrelativistic regime where the Gaussian distribution was also used for modeling the mesoscopic target. We show that, for the limit of small or large target size σ_b, this amplitude reduces to the single-atom (44) or the macroscopic (59) scattering amplitudes, respectively. By comparing the mesoscopic and the macroscopic amplitudes, we explore the transition between the mesoscopic and the macroscopic target scattering behavior and observe how the sensitivity to the angular momentum disappears. This phenomenon can be used to estimate the twisted electron orbital angular momentum in the experiment.
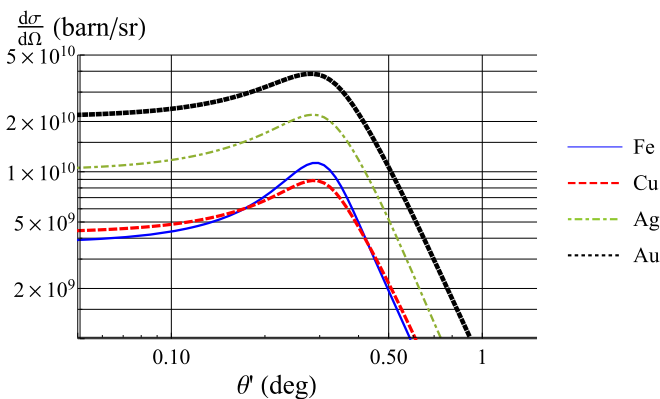

FIG. 5. The cross section for the macroscopic target made of different elements: iron, copper, silver, and gold. Parameters: $\varepsilon = 5m_e$, $\theta_p = 0.3°$ ($\kappa = 13.1$ keV).

In Fig. 3 we plot the ratio (61) as a function of the target size σ_b for different transverse momentum κ of the incident electron. The curve corresponding to $m - \lambda = 0$ is different from the others because the zero-order Bessel function behaves distinctly. Since $J_{m-\lambda}(0) = \delta_{m-\lambda,0}$, the wave function with the zero OAM interacts with a small target in its center, while for nonzero values of the OAM, the target "goes through" the wave beam center without overlapping its probability density. In (61) this can also be seen directly because the modified Bessel function with small argument behaves similarly when in it has zero index.

In Fig. 3, for every curve we can observe an evolution from left (small target size) to right (wide target) as an electron beam goes from the "single atom" scattering scenario, through the mesoscopic scattering and, finally, to the macroscopic scattering scenario. It can be seen from the single-atom scattering (49) that, for $m - \lambda \neq 0$ and when the target is on the propagation axis (impact parameter $\mathbf{b}_0 = 0$), the scattering amplitude is equal to zero, which explains the smaller values on the left side of the curves. For the macroscopic target, there is no dependence on the orbital angular momentum $m - \lambda$, so all curves converge to unity in the right part of this figure.

V. DISCUSSION AND CONCLUSION

In this paper, we show how the scattering by a screened Coulomb potential can be used to analyze the properties of the twisted relativistic electron beams. The scattering by a macroscopic target allows us to measure the transverse momentum κ (and the beam cone angle θ_p) under a condition that κ has values of at least 10 keV. The electrons with such high transverse momenta can, in principle, be generated via scattering processes at accelerator facilities, especially when employing the generalized measurement technique [22].

Moreover, we demonstrate how a target of a finite size (*mesoscopic*) can be used to retrieve information about the twisted electron orbital angular momentum $m - \lambda$. Our method allows us to estimate the electron OAM by taking targets of different sizes σ_b and analyzing the ratio $\mathcal{R}_{m-\lambda}(\sigma_b, \kappa)$ of the number of events for mesoscopic and macroscopic targets, assuming the electron transverse momentum κ is known. For $\kappa \sim 40$ eV, the OAM of any value can be retrieved for realistic targets wider than 1 nm. In contrast, for higher values of κ, the scattering process is sensitive only to higher values of the OAM for such targets, for $\kappa = 4.4$ keV, we can distinguish $m - \lambda$ starting from 50 and higher. For $\kappa = 44$ keV, the lowest retrievable value of OAM is $m - \lambda = 500$. In general, for high-enough transverse momentum ($\kappa \gtrsim 1$ keV) there is a

restrictive bottom bound in the range of measurable OAM values for the realistic target sizes ($\gtrsim 1$ nm). Increasing κ leads to a rise of this bottom bound value. However, the proposed method does not, in principle, impose an upper bound on the OAM value we can possibly measure.

To conclude, we estimate the sensitivity of the proposed OAM measurement method. Let us consider two values of the OAM $m_2 - \lambda_2$ and $m_1 - \lambda_1$, which we wish to distinguish, and introduce the following relations:

$$\delta = \frac{(m_2 - \lambda_2) - (m_1 - \lambda_1)}{m_2 - \lambda_2}, \tag{67}$$

$$\mathcal{D} = \max_{\sigma_b, \kappa \in \mathbb{R}_+} [\mathcal{R}_{m_2 - \lambda_2}(\sigma_b, \kappa) - \mathcal{R}_{m_1 - \lambda_1}(\sigma_b, \kappa)], \tag{68}$$

where $m_2 - \lambda_2 > m_1 - \lambda_1$. The relation δ characterizes the OAM detuning and the function $\mathcal{D}$ quantifies the necessary accuracy in the scattering amplitude measurement. If there is a two times difference between the OAM values ($\delta = 0.5$) we have $\mathcal{D} \approx 0.45$. For closer OAM values (smaller δ), $\mathcal{D}$ also decreases: for $\delta \approx 0.08$ we have $\mathcal{D} \approx 0.064$, and for $\delta \approx 0.01$ we have $\mathcal{D} \approx 0.007$. For example, to distinguish $m_1 - \lambda_1 = 11$ and $m_2 - \lambda_2 = 12$ (detuning $\delta = 0.083$) we must have the experimental setup resolution better than $\mathcal{D} = 0.064$. We notice that $\mathcal{D}$ and δ are of the same order of magnitude. We can use this fact at a preliminary stage of experiment planning.

ACKNOWLEDGMENTS

APPENDIX A: NORMALIZATION OF WAVE FUNCTIONS

The plane-wave normalization is introduced as follows:

$$\psi^{PW} = N^{PW} u_{\mathbf{p}\lambda} e^{ipx}. \tag{A1}$$

The wave function should obey a normalization condition on $\rho = j_0$, $\int_V d^3r\, \rho(\mathbf{r}) = 1$. That results in

$$N^{PW} = \frac{1}{\sqrt{2\varepsilon V}}. \tag{A2}$$

Let us follow the same steps to find the normalization constant of the twisted wave function

$$\psi_{\kappa m p_z \lambda}(\mathbf{r}) = N^{TW} \int \frac{d^2 p_\perp}{(2\pi)^2} a_{\kappa m}(\mathbf{p}_\perp) \psi_{\mathbf{p}\lambda}. \tag{A3}$$

Using $\int_0^R J_n^2(\kappa r) \kappa r\, dr = \frac{R}{\pi}$ ([31]), we find

$$N^{TW} = \sqrt{\frac{\pi}{2\varepsilon R L_z}}. \tag{A4}$$

We could also regularize the twisted wave-function density employing the Gaussian distribution $\exp{-1/2(r/\sigma)^2}$. Then we have

$$\kappa \int_0^R J_n^2(\kappa r) e^{-\frac{1}{2}\left(\frac{r}{\sigma}\right)^2} r\, dr = 2\pi\sigma^2 \kappa e^{-\sigma^2\kappa^2} I_n(\sigma^2\kappa^2). \tag{A5}$$

For a large value of σ there is a limit [see Eq. (55)] for the Bessel function reducing the expression above to $\sqrt{2\pi}\sigma$. In this case, the normalization constant is

$$N^{TW,reg} = \sqrt{\frac{1}{2\varepsilon\sqrt{2\pi}\sigma L_z}}. \tag{A6}$$

Therefore, we can interpret R in (A4) as a Bessel beam width.

APPENDIX B: EVALUATION OF THE INTEGRALS WITH METHOD OF STATIONARY PHASE

For small κb, the integral (20) can be easily evaluated numerically. However, for large κb the integral becomes highly oscillatory making the calculation much harder. However, the method of the stationary phase [28,29] is applicable in this limit. This method is used to evaluate integrals of the following form:

$$F(\lambda) = \int_a^b f(x) \exp[i\lambda S(x)] dx, \tag{B1}$$

where $\lambda \gg 1$ is a large parameter. The point x_0 where $S'(x) = 0$ is called a stationary point. If $[S''(x_0) \neq 0]$, we have the following approximation:

$$F(\lambda; x_0) = \sqrt{\frac{2\pi}{\lambda |S''(x_0)|}} [f(x_0) + O(\lambda^{-1})]$$

$$\times \exp\left[i\lambda S(x_0) + \frac{i\pi}{4} \text{sgn}\, S''(x_0)\right]. \tag{B2}$$

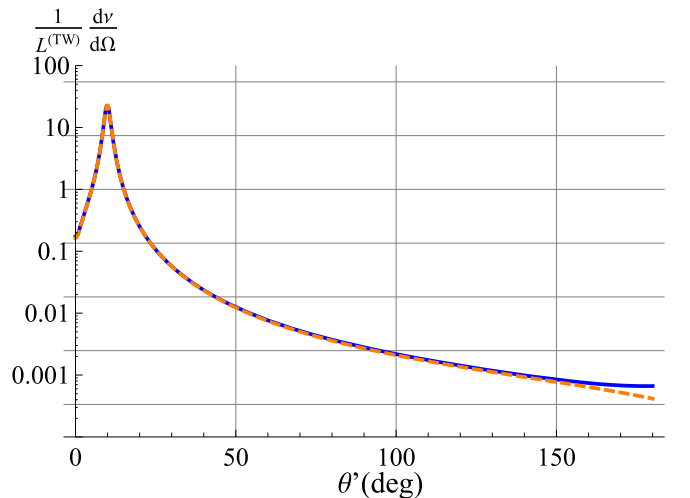Let us see how this method can be applied to the integral (20) [in principle, it also can be used for (C3)]. In terms of

FIG. 6. The number of events for the hydrogen single-atom target. $\varepsilon = 2m_e$, $\theta_p = 10°$ ($\kappa = 154$ keV), $b = 1$ nm, $m = 3/2$, $\lambda = 1/2$. Blue solid line: numerical calculation; orange dashed line: method of stationary phase.

(B1) the parameters are $\lambda = \kappa b$, $x = \phi$. If $n \ll \kappa b$, then we can take

$$S(x) = -\cos(\phi + \varphi' - \varphi_b), \tag{B3}$$

$$f(x) = \frac{1}{2\pi} \frac{e^{in\phi}}{\alpha - \beta \cos \phi}. \tag{B4}$$

Here $S'(x) = \sin(\phi + \varphi' - \varphi_b)$ and it equals to zero if $\phi = \varphi_b - \varphi'$ or $\phi = \varphi_b - \varphi' + \pi$, thus we have two stationary points. Using (B2), we find the stationary phase approximation for (20)

$$\mathcal{I}_n(\alpha, \beta, \mathbf{b}) \approx \sqrt{\frac{1}{2\pi \kappa b}} \left[\frac{e^{in(\varphi_b - \varphi')} e^{-i(\kappa b - \frac{\pi}{4})}}{\alpha - \beta \cos(\varphi_b - \varphi')} \right.$$
$$\left. - \frac{e^{in(\varphi_b - \varphi')} e^{i(\kappa b - \frac{\pi}{4})}}{\alpha + \beta \cos(\varphi_b - \varphi')} \right]. \tag{B5}$$

In Fig. 6 we compare a straightforward numerical calculation and the stationary phase approximation for the calculation

of the number of events for a single-atom target (48). We see that the curves coincide everywhere except the regions where the function becomes too small. The accuracy of the method can be roughly estimated as $(\kappa b)^{-1}$. To obtain higher accuracy we can take the next terms in approximation series, see, for example, [28].

If $n \sim \kappa b$, then $e^{in\phi}$ also oscillates fast, so we should take the following relations instead:

$$S(x) = \frac{n}{\kappa b} - \cos(\phi + \varphi' - \varphi_b), \tag{B6}$$

$$f(x) = \frac{1}{2\pi} \frac{1}{\alpha - \beta \cos \phi}. \tag{B7}$$

The next steps are obvious. Note, however, the points where $S''(x) = 0$ in which another formula for the method of stationary phase should be used (see [28,29]).

APPENDIX C: FORMULAS ON THE MESOSCOPIC TARGET SCATTERING

We present below calculations of mesoscopic scattering amplitude and number of events. The full representation of (51) is

$$\left| F_{m,\lambda,\lambda'}^{(\text{meso})}(\mathbf{p}, \mathbf{p}', \mathbf{b}_0) \right|^2 = \int d^2b \, |F(\mathbf{p}, \mathbf{p}', \mathbf{b})|^2 \frac{e^{-\frac{1}{2}\left(\frac{\mathbf{b}-\mathbf{b}_0}{\sigma_b}\right)^2}}{2\pi \sigma_b^2}$$

$$= \int \frac{d^2k_\perp}{(2\pi)^2} \frac{d^2p_\perp}{(2\pi)^2} d^2b \, f_{\lambda,\lambda'}(\mathbf{p}, \mathbf{p}') f_{\lambda,\lambda'}^*(\mathbf{k}, \mathbf{p}') a_{\kappa m}(\mathbf{p}_\perp) a_{\kappa m}^*(\mathbf{k}_\perp) e^{i(\mathbf{k}_\perp - \mathbf{p}_\perp)\mathbf{b}} \frac{e^{-\frac{1}{2}\left(\frac{\mathbf{b}-\mathbf{b}_0}{\sigma}\right)^2}}{2\pi \sigma_b^2}. \tag{C1}$$

The twisted amplitude (19) can be inserted here straightforwardly, but it is more instructive to expand the equation above as follows:

$$\int \left| F_{\lambda,\lambda'}^{(m)}(\mathbf{p}, \mathbf{p}', \mathbf{b}) \right|^2 \frac{1}{2\pi \sigma_b^2} e^{-\frac{1}{2}\left(\frac{\mathbf{b}-\mathbf{b}_0}{\sigma_b}\right)^2} d^2b = \frac{\kappa}{2\pi} \int \frac{d\varphi_k}{2\pi} \frac{d\varphi_p}{2\pi} e^{im(\varphi_p - \varphi_k)} f_{\lambda,\lambda'}(\mathbf{p}_\kappa, \mathbf{p}') f_{\lambda,\lambda'}^*(\mathbf{k}_\kappa, \mathbf{p}') e^{-\sigma^2 \kappa^2 (1 - \cos(\varphi_k - \varphi_p))} e^{i\kappa|\mathbf{b}_0|\cos(\varphi_k - \varphi_b)}$$

$$\times e^{-i\kappa|\mathbf{b}_0|\cos(\varphi_p - \varphi_b)} = \frac{2Z^2 e^4}{\pi} \kappa \left(\varepsilon^2 \delta_{\lambda,\lambda'} + m_e^2 \delta_{\lambda,-\lambda'} \right)$$

$$\times e^{-\sigma_b^2 \kappa^2} \sum_{\sigma,\sigma'=\pm 1/2} d_{\sigma,\lambda}^{1/2}(\theta_p) d_{\sigma,\lambda'}^{1/2}(\theta') d_{\sigma',\lambda}^{1/2}(\theta_p) d_{\sigma',\lambda'}^{1/2}(\theta') \mathcal{I}_{m\sigma\sigma'}^{\sigma_b}(\alpha, \beta, \mathbf{b}_0), \tag{C2}$$

where we used the property that the Fourier transform of a Gaussian is a Gaussian itself and introduced

$$\mathcal{I}_{m\sigma\sigma'}^{\sigma_b}(\alpha, \beta, \mathbf{b}_0) = \int \frac{d\varphi_p}{2\pi} \frac{e^{im\varphi_p} e^{i\sigma(\varphi' - \varphi_p)} e^{-i\kappa|\mathbf{b}_0|\cos(\varphi_p - \varphi_b)}}{\alpha - \beta \cos(\varphi_p - \varphi')} \left(\int \frac{d\varphi_k}{2\pi} \frac{e^{im\varphi_k} e^{i\sigma'(\varphi' - \varphi_k)} e^{-i\kappa|\mathbf{b}_0|\cos(\varphi_k - \varphi_b)}}{\alpha - \beta \cos(\varphi_k - \varphi')} e^{\sigma_b^2 \kappa^2 \cos(\varphi_k - \varphi_p)} \right)^*. \tag{C3}$$

This integral has similar calculation issues to the integral of (20). Let us see how it behaves in the limit of small θ_p and β while setting $\mathbf{b}_0 = 0$:

$$\mathcal{I}_{m\sigma\sigma'}^{\sigma_b}(\alpha, 0, 0) = \int \frac{d\varphi_p}{2\pi} \frac{e^{im\varphi_p} e^{i\sigma(\varphi' - \varphi_p)}}{\alpha} \left(\int \frac{d\varphi_k}{2\pi} \frac{e^{im\varphi_k} e^{i\sigma'(\varphi' - \varphi_k)} e^{\sigma_b^2 \kappa^2 \cos(\varphi_k - \varphi_p)}}{\alpha} \right)^*$$

$$= \frac{1}{\alpha^2} \delta_{m-\sigma, m-\sigma'} i^{-(m-\sigma')} J_{m-\sigma'}\left(i\sigma_b^2 \kappa^2\right)$$

$$= \frac{1}{\alpha^2} \delta_{\sigma,\sigma'} I_{m-\sigma}\left(\sigma_b^2 \kappa^2\right), \tag{C4}$$

where $I_{m-\sigma}(\sigma_b^2\kappa^2)$ is a modified Bessel function of the first kind. In this limit we find for the amplitude (C2)

$$\int \left|F_{\lambda,\lambda'}^{(m)}(\mathbf{p},\mathbf{p}',\mathbf{b})\right|^2 \frac{1}{2\pi\sigma_b^2} e^{-\frac{1}{2}\left(\frac{\mathbf{b}}{\sigma_b}\right)^2} d^2b = \frac{2Z^2e^4}{\pi}\kappa\left(\varepsilon^2\delta_{\lambda,\lambda'} + m_e^2\delta_{\lambda,-\lambda'}\right)e^{-\sigma_b^2\kappa^2}\sum_{\sigma=\pm 1/2}\left(d_{\sigma,\lambda}^{1/2}(\theta_p)d_{\sigma,\lambda'}^{1/2}(\theta')\right)^2\frac{1}{\alpha^2}I_{m-\sigma}\left(\sigma_b^2\kappa^2\right)$$

$$= \frac{2Z^2e^4}{\pi}\kappa\left[\varepsilon^2\cos(\theta'/2)\delta_{\lambda,\lambda'} + m_e^2\sin(\theta'/2)\delta_{\lambda,-\lambda'}\right]e^{-\sigma_b^2\kappa^2}\frac{1}{\alpha^2}I_{m-\lambda}\left(\sigma_b^2\kappa^2\right). \qquad (C5)$$

In addition, for the number of events we have

$$\left(\frac{d\nu}{d\Omega}\right)^{(\mathrm{meso})} = \frac{N_e}{16\pi^2}\frac{|\mathbf{p}|}{\varepsilon}\left|F_{m,\lambda,\lambda'}^{(\mathrm{meso})}(\mathbf{p},\mathbf{p}',\mathbf{b}_0)\right|^2$$

$$= 2Z^2e^4\frac{\kappa}{R}\frac{N_e}{\cos\theta_p}\left(\varepsilon^2\delta_{\lambda,\lambda'} + m_e^2\delta_{\lambda,-\lambda'}\right)e^{-\sigma_b^2\kappa^2}\sum_{\sigma,\sigma'=\pm 1/2}d_{\sigma,\lambda}^{1/2}(\theta_p)d_{\sigma,\lambda'}^{1/2}(\theta')d_{\sigma',\lambda}^{1/2}(\theta_p)d_{\sigma',\lambda'}^{1/2}(\theta')\mathcal{I}_{m\sigma\sigma'}^{\sigma_b}(\alpha,\beta,\mathbf{b}_0). \qquad (C6)$$

[1] J. Torres and L. Torner, *Twisted Photons: Applications of Light with Orbital Angular Momentum* (John Wiley & Sons, New Jersey, 2011).

[2] I. P. Ivanov and V. G. Serbo, Phys. Rev. A **84**, 033804 (2011).

[3] K. Bliokh, I. Ivanov, G. Guzzinati, L. Clark, R. Van Boxem, A. Béché, R. Juchtmans, M. Alonso, P. Schattschneider, F. Nori, and J. Verbeeck, Phys. Rep. **690**, 1 (2017).

[4] M. Uchida and A. Tonomura, Nature (London) **464**, 737 (2010).

[5] J. Verbeeck, H. Tian, and P. Schattschneider, Nature (London) **467**, 301 (2010).

[6] B. J. McMorran, A. Agrawal, I. M. Anderson, A. A. Herzing, H. J. Lezec, J. J. McClelland, and J. Unguris, Science **331**, 192 (2011).

[7] V. Grillo, G. C. Gazzadi, E. Mafakheri, S. Frabboni, E. Karimi, and R. W. Boyd, Phys. Rev. Lett. **114**, 034801 (2015).

[8] E. Mafakheri, A. H. Tavabi, P.-H. Lu, R. Balboni, F. Venturi, C. Menozzi, G. C. Gazzadi, S. Frabboni, A. Sit, R. E. Dunin-Borkowski, E. Karimi, and V. Grillo, Appl. Phys. Lett. **110**, 093113 (2017).

[9] B. McMorran, A. Agrawal, P. Ercius, V. Grillo, A. Herzing, T. Harvey, and M. Linck, Phil. Trans. R. Soc. A **375**, 20150434 (2017).

[10] A. Plumadore and A. L. Harris, J. Phys. B **53**, 205205 (2020).

[11] A. L. Harris, A. Plumadore, and Z. Smozhanyk, J. Phys. B **52**, 094001 (2019).

[12] N. Dhankhar, A. Mandal, and R. Choubisa, J. Phys. B **53**, 155203 (2020).

[13] S. M. Lloyd, M. Babiker, and J. Yuan, Phys. Rev. A **86**, 023816 (2012).

[14] S. Lloyd, M. Babiker, and J. Yuan, Phys. Rev. Lett. **108**, 074802 (2012).

[15] V. Serbo, I. P. Ivanov, S. Fritzsche, D. Seipt, and A. Surzhykov, Phys. Rev. A **92**, 012705 (2015).

[16] V. P. Kosheleva, V. A. Zaytsev, A. Surzhykov, V. M. Shabaev, and T. Stöhler, Phys. Rev. A **98**, 022706 (2018).

[17] D. V. Karlovets, G. L. Kotkin, and V. G. Serbo, Phys. Rev. A **92**, 052703 (2015).

[18] D. V. Karlovets, G. L. Kotkin, V. G. Serbo, and A. Surzhykov, Phys. Rev. A **95**, 032703 (2017).

[19] R. Van Boxem, B. Partoens, and J. Verbeeck, Phys. Rev. A **89**, 032715 (2014).

[20] R. Van Boxem, B. Partoens, and J. Verbeeck, Phys. Rev. A **91**, 032703 (2015).

[21] D. Karlovets, New J. Phys. **23**, 033048 (2021).

[22] D. V. Karlovets, S. S. Baturin, G. Geloni, G. K. Sizykh, and V. G. Serbo, Eur. Phys. J. C **82**, 1008 (2022).

[23] I. P. Ivanov, Prog. Part. Nucl. Phys. **127**, 103987 (2022).

[24] A. I. Akhiezer and V. B. Berestetskii, *Quantum Electrodynamics*, Interscience Monographs and Texts in Physics and Astronomy, Vol. 11 (John Wiley & Sons, New Jersey, 1965).

[25] V. B. Berestetskii, E. M. Lifshitz, and L. P. Pitaevskii, *Quantum Electrodynamics*, Course of Theoretical Physics, Vol. 4 (Pergamon, Oxford, UK, 1982).

[26] D. A. Varshalovich, A. N. Moskalev, and V. K. Khersonskii, *Quantum Theory of Angular Momentum* (World Scientific, Singapore, 1988).

[27] Sometimes this kind of potential is called the Yukawa potential because it has the same functional form.

[28] M. V. Fedoryuk, *The Saddle-Point Method* (Nauka, Moscow, 1977).

[29] C. Bender and S. Orszag, *Advanced Mathematical Methods for Scientists and Engineers I: Asymptotic Methods and Perturbation Theory*, Advanced Mathematical Methods for Scientists and Engineers (Springer, New York, 1999).

[30] D. V. Karlovets and V. G. Serbo, Phys. Rev. Lett. **119**, 173601 (2017).

[31] U. D. Jentschura and V. G. Serbo, Eur. Phys. J. C **71**, 1571 (2011).

[32] F. Salvat, J. D. Martinez, R. Mayol, and J. Parellada, Phys. Rev. A **36**, 467 (1987).

[33] D. V. Karlovets and V. G. Serbo, Phys. Rev. D **101**, 076009 (2020).

[34] M. D. Schwartz, *Quantum Field Theory and the Standard Model* (Cambridge University Press, Cambridge, England, 2014).

[35] H. Ott, Rep. Prog. Phys. **79**, 054401 (2016).

[36] J. Verbeeck, P. Schattschneider, S. Lazar, M. Stöger-Pollach, S. Löffler, A. Steiger-Thirsfeld, and G. Van Tendeloo, Appl. Phys. Lett. **99**, 203109 (2011).

[37] P. Schattschneider, S. Löffler, M. Stöger-Pollach, and J. Verbeeck, Ultramicroscopy **136**, 81 (2014).

[38] https://rscf.ru/en/project/23-62-10026/.

Correction: Formatting errors were introduced during the proof cycle in Eqs. (23), (25), (32), and (44) and have been fixed.